Macroscopic Magnetic Coupling Effect: The Physical Origination of a High-Temperature Superconducting Flux Pump

Wei Wang[1,*] and Tim Coombs[2]

[1]College of Electrical Engineering and Information Technology, Sichuan University, Chengdu 610065, People's Republic of China

[2]Electrical Engineering Division, Department of Engineering, University of Cambridge, Cambridge CB3 0FA, United Kingdom

(Received 18 August 2017; revised manuscript received 30 August 2017; published 17 April 2018; corrected 9 May 2018)

We have uncovered at the macroscopic scale a magnetic coupling phenomenon in a superconducting $YBa_2Cu_3O_{7-\delta}$ (YBCO) film, which physically explains the mechanism of the high-temperature superconducting flux pump. The coupling occurs between the applied magnetic poles and clusters of vortices induced in the YBCO film, with each cluster containing millions of vortices. The coupling energy is verified to originate from the inhomogeneous field of the magnetic poles, which reshapes the vortex distribution, aggregates millions of vortices into a single cluster, and accordingly moves with the poles. A contrast study is designed to verify that, to provide the effective coupling energy, the applied wavelength must be short while the field amplitude must be strong, i.e., local-field inhomogeneity is the crucial factor. This finding broadens our understanding of the collective vortex behavior in an applied magnetic field with strong local inhomogeneity. Moreover, this phenomenon largely increases the controlled vortex flow rate by several orders of magnitude compared with existing methods, providing motivation for and physical support to a new branch of wireless superconducting dc power sources, i.e., the high-temperature superconducting flux pump.

DOI: 10.1103/PhysRevApplied.9.044022

I. INTRODUCTION

Magnetic flux enters a type-II superconductor as quantized magnetic vortices, each carrying magnetic flux quantum $\Phi_0 = h/2e = 2.07 \times 10^{-15}$ Wb. For vortices penetrating into a superconducting sample, there are three major forces that determine the vortex movement: the pinning force F_p arising from defects in the superconductor, the repulsive force F_v between vortices of the same sign, and the attractive image force F_b between the vortex and the sample edge. This last force originates from the boundary condition stating that no current leaves the boundary and is satisfied by adding an image vortex of the opposite sign [1–3]. This image force provides a boundary energy barrier to vortex penetration and may have a long-range interaction in superconducting thin films [4,5]. The pinning force F_p prohibits the vortex from free movement in the superconducting sample. However, the mutual repulsive forces F_v between vortices of the same sign drives the vortices into motion when $F_v > F_p$. This mutual repulsive force arranges the vortices into the characteristic regular triangular lattice with spacing $a = \{2\Phi_0/[(3)^{1/2}B]\}^{1/2}$. The classic magnetization models for the type-II superconducting materials with strong pinning, such as the Bean model [6], have assumed critical values for the magnetic gradient as a result of the force balance between the collective mutual repulsive force and the pinning force, i.e., $F_v = F_p$. To date, the Bean model provides a powerful means to predict the magnetization behavior in type-II superconducting materials in homogeneous oscillating fields.

Because of the microscopic scale of the vortices and the strong pinning effect, controlling the vortex motion in a superconducting film remains technically challenging. Nevertheless, such control has important scientific and technological implications, such as for fluxon "pumps," "lenses," and "diodes." To date, there are two distinct ways to control the vortex motion in type-II superconducting films; one is based on the "ratchet effect" [7,8], the other is the "dc transformer" [9]. The ratchet effect is based on artificial asymmetric pinning centers in the superconducting film to rectify the vortex flow direction in ac stimulation. By applying an ac current, the flow rate is higher in one direction than the opposite, causing a net vortex flow in the favored direction and outputs a dc voltage. The profiles of these artificial asymmetric pinning potentials include the sawtooth [10,11] and triangular [7,12] shapes. In layered superconductors such as YBCO and $Bi_2Sr_2CaCu_2O_{8+\delta}$, the ratchet effect can be induced by the interactive forces between Josephson vortices and pancake vortices [13,14].

*Corresponding author.
weiwangca283@gmail.com

Giaever's pioneering work on the dc transformer has showed that the vortex motion can be controlled via vortex-vortex coupling [9,15]. In his experiments, two superconducting films—a primary and a secondary—were superposed and electrically insulated. The thicknesses of both superconducting layers were several thousand angstroms, whereas the thickness of the insulation layer was several hundred angstroms. A dc background field was applied perpendicularly to the superconducting films to establish an Abrikosov vortex lattice in both superconducting layers. The noted effect was the mutual attractive force between paired vortices, one located in the primary film and the other located in the secondary film. The force tended to line up the two vortices, thus inducing a vortex-vortex coupling [16]. If a vortex flow is triggered in the primary film by injecting a dc current, for example, the vortex of the coupled pair in the secondary film flows accordingly, and thereby produces dc voltages in both superconducting layers. A similar effect is also found in the intermediate states of type-I superconducting films [17]. In the layered superconductor, this coupling between paired pancake vortices in different CuO_2 layers plays an important role in its vortex dynamics [18].

In the dc transformer, the vortex-vortex coupling force arises from field inhomogeneity existing in the vortex structure [19]. Experiments have shown that, as a result of field smoothing, increasing the vortex density [19,20] or the thickness of the insulation layer [21,22] reduces the coupling force. In particular, the coupling force rapidly diminishes when the vortex spacing a is comparable to the thickness of the insulation layer because the field becomes strongly homogeneous [23,24]. The coupling energy $E_c(\vec{s})$ can be derived from the Gibbs free energy [23–25]. Its minimum value occurs when the primary vortex lattice overlaps with the secondary lattice; its maximum value occurs when the primary vortices are beneath the centers of the equilateral triangles of the secondary vortex lattice [24]. Therefore, the coupling energy is periodic [23,24]. The coupling force is derived from the gradient of $E_c(\vec{s})$ [24], $\vec{F}_c(\vec{s}) = \nabla_s E_c(\vec{s})$. Therefore, misaligning the two coupled vortices results in a coupling force as it increases the coupling energy.

In light of the foregoing, we consider the possibility of inducing a magnetic coupling effect at the macroscopic scale by applying a magnetic pole of a relatively short wavelength. If the coupling is possible at this scale, the coupling length should increase from a microscopic 10^{-7} m in the dc transformer to a macroscopic 10^{-2} m. The coupling is between a single applied pole and millions of vortices in the superconducting film, separate from the single vortex-vortex coupling in the dc transformer. Hence, this coupling increases significantly the controlled vortex flow rate and eases the control complexity.

The content of this work is arranged as follows. First, we introduce the experimental setup and the numerical method. Second, based on the numerical model which is verified in experiments, we compare the vortex behavior inside a YBCO thin, which is magnetized by the magnetic poles of different wavelengths, and establish that the macroscopic magnetic coupling requires short-wavelength conditions. We next discuss the impact of the field amplitude on the coupling effect. Finally, we discuss the impact of this finding on practical applications; in particular, we fully explain the HTS flux pump behavior based on our finding.

II. EXPERIMENTAL AND SIMULATION TECHNIQUES

In this work, we apply magnetic poles with wavelengths comparable to the size of the superconducting sample. Hence, the local-field inhomogeneity is strong in the superconducting region. Also, to observe the magnetization process clearly and to avoid geometric interference, we chose a circular shape for both the sample and the applied poles. To address the foregoing concerns, a device, referred to as a "circular-type magnetic flux pump" (CTMFP) [26–32], is fabricated; its structure is shown in Fig. 1(a). The device generates short-wavelength magnetic poles, which are axisymmetric [Fig. 1(b)]. The applied field is normal to the surface of the round $YBa_2Cu_3O_{7-\delta}$ film (prepared by Ceraco Ceramic Coating GmbH, Germany) [28]. Although the CTMFP devices generate an ac field, the experimental principle is different from the conventional ac susceptibility measurements in alternating fields [33,34] and rotating fields [35–38], or the magneto-optical studies of flux penetration [39] and avalanches [40] in ac fields. The studies of the latter involved experiments using uniform fields rather than fields of strong inhomogeneity.

The YBCO film is 50 mm in diameter; the thickness of the YBCO layer is 2000 Å, which is about one-fifth of a commercial coated conductor (CC) of high-temperature superconducting (HTS) material. The YBCO layer is deposited on a 2-in.-diameter Al_2O_3 wafer. The sample is sealed inside a Tufnol chamber to protect it from humidity and scratches. Fifteen Hall sensors are installed above the sample to measure the flux densities along the radius. During the experiments, the whole device [Fig. 1(a)] is submerged in liquid nitrogen at 77 K to maintain the YBCO film in the superconducting state.

The numerical simulation is based on the finite-element method (FEM) applying Maxwell's equations and the nonlinear $E-J$ power relation of the YBCO sample. The governing equation is expressed as [26,27,29]

$$\mu_r\mu_0\frac{\partial \boldsymbol{H}}{\partial t} + \nabla \times (\rho \nabla \times \boldsymbol{H}) = 0, \tag{1}$$

for which the magnetic field $\boldsymbol{H} = [H_r, H_z]^T$ is given in cylindrical coordinates; the E-J power law gives the resistivity of the sample, $\rho = J^{n-1}E_C/J_C^n$, with critical current density $J_C = 1.87$ MA/cm^2, which is comparable to a commercial 2G HTS CC; the index value $n = 30$, and

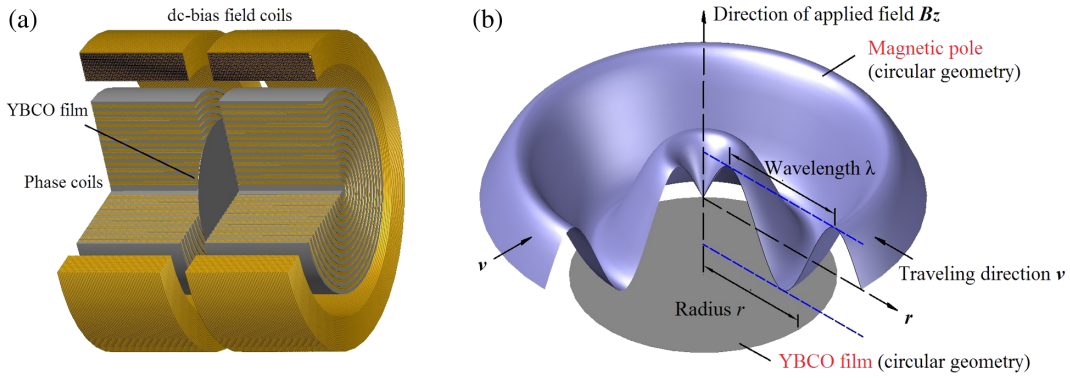

FIG. 1. (a) CTMFP experimental device contains two identical CTMFP magnets, each comprising phase windings in the center and a dc coil in the outer periphery. A round YBCO film is sandwiched in the gap between the two magnets. The function of the device is to generate short-wavelength magnetic poles that are axisymmetric. (b) The short-wavelength magnetic poles generated by the device are axisymmetric with the applied field normal to the sample surface. The traveling direction of the magnetic pole is towards the sample center.

the criterion $E_C = 10^{-4}$ V/m. The field dependence of J_C on the magnetic flux density $\boldsymbol{B}$ is not considered in the model. The model has been verified in experiments, reproducing the magnetization, and uncovers the vortex dynamics inside the YBCO film [26,27].

To describe the relative size between the sample and the applied pole [26], a dimensionless parameter $\delta = r/\lambda$, where $r = 25.0$ mm is the radius of the YBCO film and λ the wavelength of the magnetic pole. Thus, the value $[2\delta]$ indicates the number of magnetic poles in the superconducting region.

III. RESULTS AND DISCUSSION

Based on the results of the verified FEM model, we discuss the impact of the field inhomogeneity of the ac traveling wave on the magnetization of the YBCO film. The degree of field inhomogeneity derives from two aspects: wavelength and amplitude; i.e., shortening the wavelength or increasing the amplitude increases the field inhomogeneity. In the first part of the following work, we shorten the wavelength, observing the changes in magnetization behavior from the widely accepted Bean model to the unknown magnetic coupling effect. In the second part, with short-wavelength conditions, we decrease the field amplitude observing the vanishing of the coupling effect through field smoothening.

Three different wavelength conditions are chosen for our comparative study: (I) long-wavelength condition $\lambda = 250.0$ mm, $2\delta = 0.2$, derived from the FEM model; (II) short-wavelength condition $\lambda = 30.0$ mm, $2\delta = 1.7$, from the verified FEM model based on the original CTMFP device [27,28]; and (III) short-wavelength condition $\lambda = 15.0$ mm, $2\delta = 3.3$, from the verified FEM model based on an updated CTMFP device [26]. The amplitudes of the magnetic pole are all set to $B_{ac} = 2.0$ mT. Hence, only the wavelength λ affects the local-field inhomogeneity, i.e., case III has the strongest field inhomogeneity and case I the weakest. The frequencies of the ac traveling waves are all set to $f = 0.1$ Hz. The applied fields of the three different wavelengths are applied to a pristine YBCO sample. During the magnetization process, the penetrated flux inside the sample is calculated based on the verified FEM model.

The result for the long-wavelength condition I [Fig. 2(a)] shows the magnetization behavior resembles that of the Bean model. The top three curves give the applied field in the superconducting region, for transient moments $t = 0$, 0.2, 0.4 T (marked as ①, ②, ③, respectively), where T is the period. The bottom three curves plot the penetrating flux inside the YBCO sample for the same moments. From Fig. 2(a), the applied field in the superconducting region is almost homogeneous as the wavelength is relatively long. In this case, magnetic flux cannot penetrate into the central region because the amplitude of the applied field is only 2.0 mT; at least 7.0 mT is required for this to occur [28]. The applied field penetrates and oscillates in the outer ring of the sample, whereas the magnetic gradient in the penetrated region exhibits constant critical values. The above features are consistent with the classic Bean critical state model [6,41], which provides excellent predictions of the collective vortex behavior of type-II superconducting materials in an oscillating homogeneous field.

However, as we shorten the wavelength to the scale comparable to the sample size, we note a distinct feature which deviates from the classic Bean model, specifically, a small field amplitude fully penetrating the sample, and a macroscopic magnetic coupling effect. From the result for the short-wavelength condition II [Fig. 2(b)], although the field amplitude is the same as in Fig. 2(a), the magnetic flux has fully penetrated the YBCO sample. Moreover, we note that the applied magnetic pole has introduced a large amount of flux into the YBCO sample; the maximum flux density is 0.4 mT, which is about 1/5 of the applied field

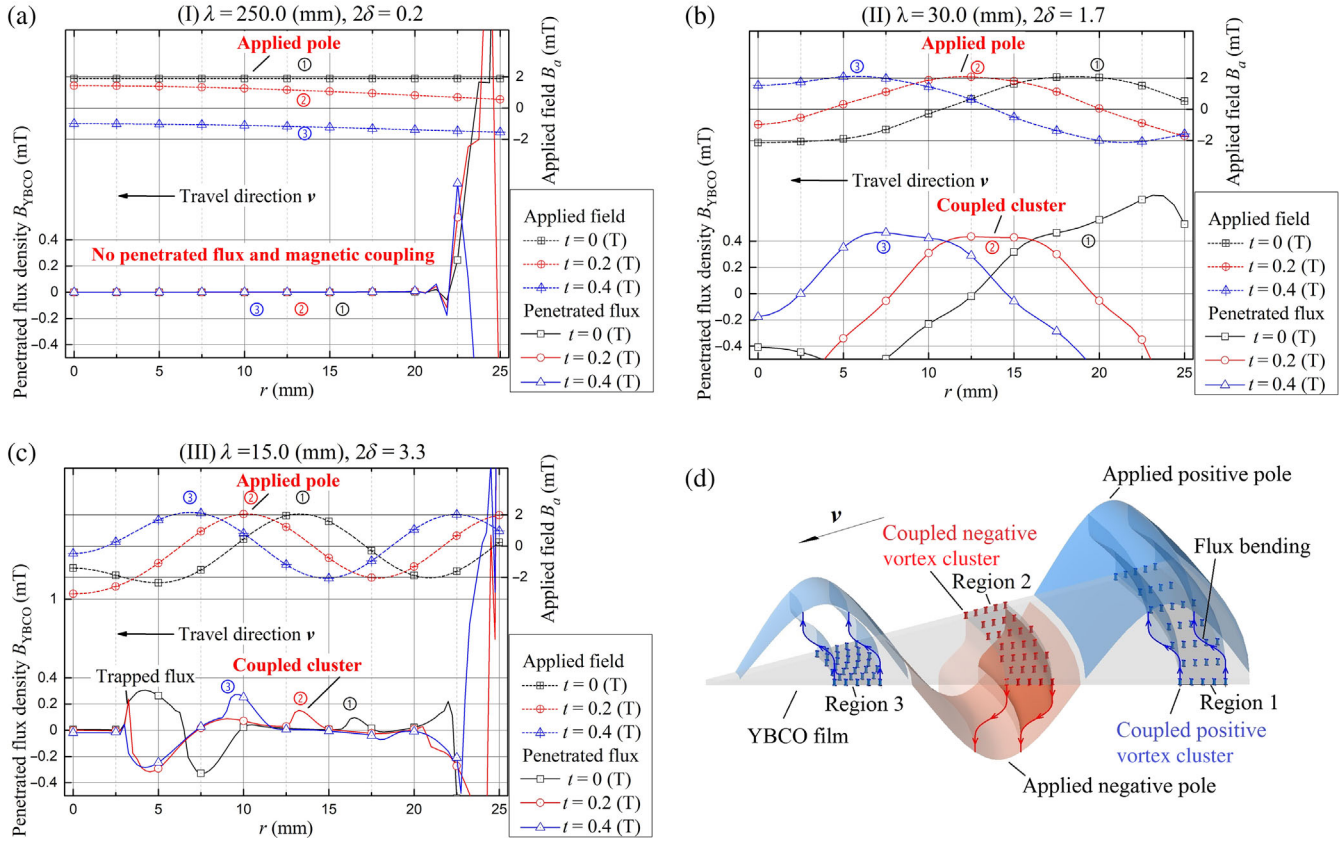

FIG. 2. (a) Long wavelength condition $\lambda = 250.0$ mm, $2\delta = 0.2$, derived from the FEM model. The top three curves show the applied field without the sample, at time $t = 0$, 0.2, 0.4 T (marked as ①, ②, ③, where T is the period); the bottom three curves show the corresponding flux densities penetrating inside the YBCO sample. (b) Short-wavelength condition $\lambda = 30.0$ mm, $2\delta = 1.7$ from the original CTMFP device. The results are derived from the FEM model. (c) Short-wavelength condition $\lambda = 15.0$ mm, $2\delta = 3.3$ from the updated CTMFP device. The results are derived from the FEM model. (d) Demonstration of coupling features revealed in Fig. 2(c), including the ramping up of vortex density and the misalignment between the applied pole and coupled cluster.

amplitude. In particular, this induced flux travels in synchrony with the applied pole; in other words, a magnetic coupling seems to have become established between the applied pole and a cluster of millions of vortices. We also note a "terrace" region in the central part of the coupled cluster that does not show critical values of the magnetic gradient. This phenomenon resembles the so-called "terraced critical state" [42,43], arising within a periodic pinning landscape, in which extremely high currents are interlaced with regions of near zero current. The terrace region [Fig. 2(b)] suggests that the periodic ac traveling wave has induced a periodic pinning potential within the vortex structure.

To further investigate this possible magnetic coupling behavior on the macroscopic scale, we further shorten the wavelength [case III]. The results [Fig. 2(c)] show that the applied magnetic pole exhibits the strongest local-field inhomogeneity. Moreover, clear magnetic coupling behavior is seen between the short-wavelength magnetic pole and the cluster of vortices. The magnetic pole induces and couples a certain number of vortices at the edge of the YBCO sample; this cluster of coupled vortices travels in synchrony with the imposed pole until it reaches the center of the YBCO sample where it remains as a trapped flux. Interestingly, during the next half period, a negative magnetic pole couples and drags a cluster of negative vortices towards the center of the YBCO sample, where it annihilates the previously trapped positive flux.

In Fig. 2(c), two clear features are apparent as the cluster travels with the applied pole. As depicted in Fig. 2(d), there is first a misalignment between the centers of the pole and cluster, when the cluster is near the rear of the pole and flux bending should be expected. Second, the flux density of the cluster ramps up as it travels from the sample edge towards the center. The misalignment between the pole and the cluster follows the theoretical prediction for the misalignment of a coupled pair of vortices in the dc transformer [24]. As illustrated in Fig. 2(d), this behavior increases the magnetic energy and results in a driving force for the coupled vortices [23–25] that assists vortices to overcome the pinning force and travels with the applied pole.

The ramping up of the flux density can be explained from the circular geometry [Fig. 2(d)]; as the coupled vortices are confined to a certain region near the rear part of

the pole, then if the coupled vortices are transported towards the center (from region 1 to region 3), the coupled area shrinks because of the circular geometry. However, the number of coupled vortices remains the same, resulting in the ramping up of the vortex density. The confinement of vortices to isolated islands is observed in the superconducting-ferromagnet bilayer [44,45], in which the magnetic domains in the ferromagnetic layer create a pinning potential for the vortices. The difference is that, in our case, the vortex cluster is not only created by the magnetic pole, but it also travels in concert with it, i.e., a coupling force F_C is introduced into the vortex dynamics. The vortex confinement and ramping up of the vortex density suggests a strong magnetic coupling in case III.

From Figs. 2(b) and 2(c), we observe macroscopic magnetic coupling effects. We also verify that the coupling strength originates from the local-field inhomogeneity produced by the magnetic poles with short wavelength; i.e., the macroscopic magnetic coupling appears only when the applied wavelength is short enough compared with the sample size. However, as we discuss above, there is another parameter, which affects the local-field inhomogeneity apart from the wavelength λ. This is the field amplitude B_{ac}. By increasing or decreasing B_{ac}, the local-field inhomogeneity is enlarged or suppressed, which may affect the coupling strength.

To understand how the field amplitude affects the coupling strength [Figs. 2(b) and 2(c)], the field amplitude B_{ac} is halved to 1.0 mT; the results are shown in Figs. 3(a) and 3(b), respectively. Comparing Figs. 3(a) and 2(b) at $\lambda = 30.0$ mm, although B_{ac} is halved, the magnetic coupling effect is still observable, except the maximum flux density of the coupled flux is one-half that of Fig. 2(b). In this case, the coupling strength decreases linearly with the applied field. However, comparing Figs. 3(b) and 2(c) at $\lambda = 15.0$ mm, the magnetic coupling effect vanishes as B_{ac} is halved in Fig. 3(b). The applied field penetrates and oscillates in the outer ring of the sample, i.e., the YBCO sample has completely shielded the flux from entering the central region.

Note that the coupling effect vanishes in Fig. 3(b) despite the local-field inhomogeneity (shorter wavelength) being stronger than for Fig. 3(a). The result suggests that the coupling strength does not increase monotonically when shortening the wavelength λ. If the wavelength is relatively too short comparing with the sample size, the superconducting screen current smooths out the local-field inhomogeneity and weakens the coupling. This suggests that there is an optimal setting of δ for which the coupling effect is most efficient.

The macroscopic magnetic coupling effect uncovered in this work can be applied in practical applications to control massive vortex flows. Compared with single vortex-vortex coupling and transportation [9,15], this method couples and transports millions of Abrikosov vortices with each pole, thereby increasing the vortex flow rate by several orders of magnitude. Also, since our method relies on an external magnetic field, problems such as weakening coupling force through field smoothing of the high vortex density [19,20] or thick insulation layer [21,22] are avoided. Moreover, instead of using specially prepared superconducting films, commercial superconducting wire can be used with our method; difficulties such as preparing complex pinning potentials [7,8] or bilayer superconducting structures [9,15] are also avoided.

The most important applications of this finding are in helping HTS magnets to run at a persistent current mode (PCM), and in making possible flux pumping for an HTS magnet. Flux pumping is a technology that transports magnetic flux into a superconducting closed loop. For a low-temperature superconducting (LTS) magnet, this is realized by transporting flux within a normal spot in a LTS film. The normal spot is created by (i) applying a strong magnetic field (greater than critical field B_C for type-I superconducting film, or greater than upper critical field

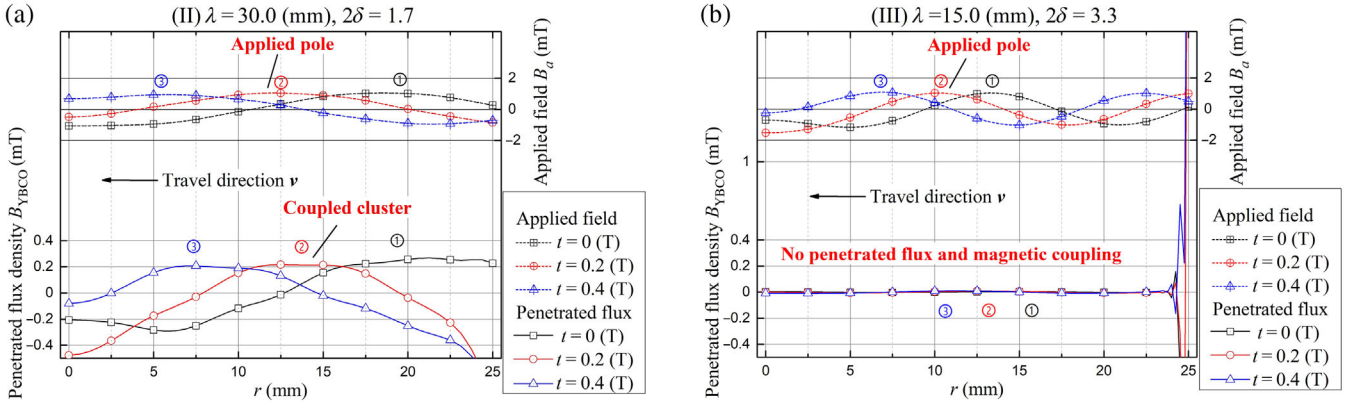

FIG. 3. (a) Short-wavelength condition $\lambda = 30.0$ mm, $2\delta = 1.7$ from the original CTMFP device, the results are derived from the FEM model. The top three curves show the applied field without the sample, at the time $t = 0$, 0.2, 0.4 T (marked as ①, ②, ③, where T is the period); the bottom three curves show the corresponding flux densities penetrating inside the YBCO sample. (b) Short-wavelength condition $\lambda = 15.0$ mm, $2\delta = 3.3$ from the updated CTMFP device. The results are derived from the FEM model.

B_{C2} for type-II superconducting film), or (ii) local heating (greater than critical temperature T_C) [46]. The normal spot is smaller than the width of the LTS film, which resembles a current switch in comparison with the superconducting region; the superconducting current bypasses the normal spot and only flows in the superconducting region. The magnetic flux is embedded in the normal spot and transported into the LTS closed loop, and eventually trapped in the LTS closed loop [46]. By repeating the process, the total flux in the LTS closed loop accumulates until the induced current reaches critical value I_C. However, for an HTS film, creating a normal spot is not practical because the upper critical field B_{C2} is very high and partially heating an HTS CC is complicated.

Based on the findings on the macroscopic magnetic coupling, the flux pumping for the HTS magnet can be achieved using vortex dynamics rather than creating a normal spot; i.e., each tiny vortex can be considered as being equivalent to a normal spot with a radius equal to the coherence length ξ and a magnetic flux equal to a magnetic flux quantum $\Phi_0 = h/2e = 2.07 \times 10^{-15}$ Wb. For a cluster with n coupled vortices, the total area of the "normal sport" equals $n\pi\xi^2$, and the total coupled flux equals $n\Phi_0$. To achieve a net flux accumulation, it is important to dc bias the ac traveling wave to suppress those magnetic poles of the undesired polarization (homopolar traveling wave only), so that only vortices of the desired spin direction are induced, coupled, and transported into the HTS closed loop during each period.

Figure 4 illustrates the mechanism for an HTS flux pump based on macroscopic magnetic coupling. In the first step [Fig. 4(a)], the homopolar traveling wave induces and couples to a vortex cluster on the outer edge of the HTS film. In the second step [Fig. 4(b)], as the magnetic pole enters the HTS closed loop, the flux line bends between the pole and the cluster, which increases the magnetic energy and behaves as a coupling force F_C, and thus drags the cluster across the HTS film. The coupling force F_C should be larger than the pinning force F_P of the HTS film, $F_C > F_P$. During the process, an induced dc voltage should be present at the terminals of the HTS film derived from

$$\boldsymbol{E} = \boldsymbol{v} \times \boldsymbol{B}_{cc}, \tag{2}$$

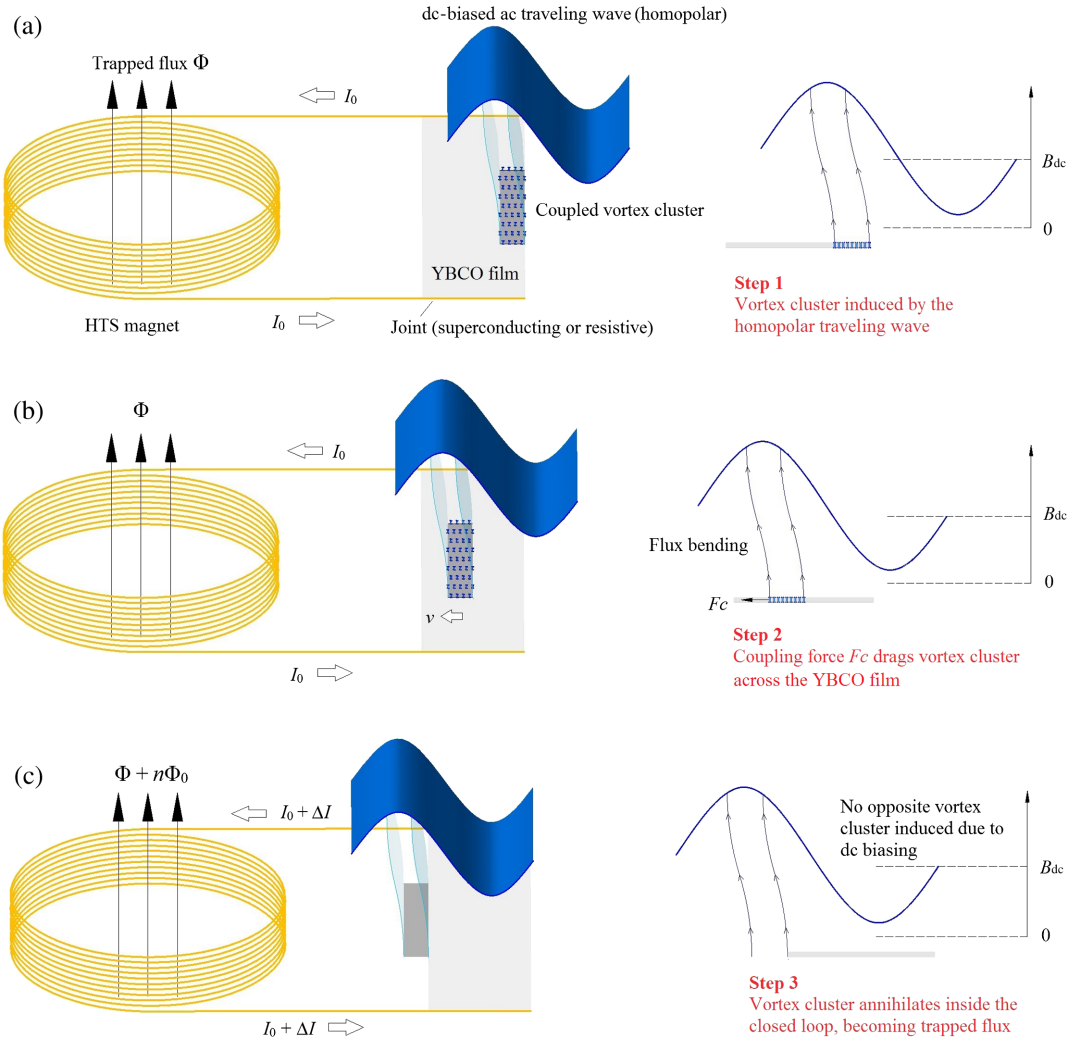

FIG. 4. Physical explanation of the HTS flux pump, based on the discovered macroscopic magnetic coupling. (a) vortex cluster induced by the homopolar traveling wave on the outer side of the YBCO film; (b) coupling force F_C drags the vortex cluster across the YBCO film; (c) vortex cluster enters the HTS closed loop, annihilates near the inner side of the HTS film, thus becoming trapped flux of the HTS magnet.

where $\boldsymbol{E}$ is the induced electric field along the longitudinal direction, $\boldsymbol{v}$ the vortex traveling direction, and $\boldsymbol{B}_{cc}$ is the flux density of the cluster. Note that only the traveling vortices induce an electric field in the HTS film.

In the third step [Fig. 4(c)], the cluster travels into the HTS closed loop and is annihilated near the inner side of the HTS film, thus forming trapped flux in the HTS magnet. The increment in the amount of flux equals the total flux of the coupled-vortex cluster, i.e.,$n\Phi_0$. As the ac traveling wave is dc biased [Fig. 4(c)], the opposite magnetic pole neither induces nor transports any opposite vortex during propagation. Hence, during each period, a net flux accumulates in the HTS closed loop. By repeating the process (Fig. 4), the HTS magnet reaches its maximum field capacity (hindered by the critical current I_C and joint resistance R_j).

The foregoing discussion clearly explains the physical origin of the HTS flux pump, based on the discovered macroscopic magnetic coupling. To date, the HTS flux pump has been widely accepted as being technically possible [47–50], except its physical origin is difficult to establish from classic superconducting electromagnetic theories [51–56]. Based on the macroscopic magnetic coupling, several predictions can be made for the HTS flux pump. (1) A pure ac traveling wave does not induce any trapped flux inside the HTS magnet, as the transported positive vortices (first half period) cancel the negative vortices (second half period) during each period. (2) The magnetization of the HTS magnet can be reversed by reversing the dc bias field of the ac traveling wave; as the polarization of the pole wave is reversed, then opposite vortices are coupled and transported into the HTS closed loop. (3) The magnetization of the HTS magnet can be reversed by reversing the propagating direction of the ac traveling wave, as trapped vortices in the HTS closed loop are transported out. The above three predictions have been experimentally proven by our latest HTS flux pump device [57], which solidifies our explanation based on macroscopic magnetic coupling.

IV. CONCLUSIONS

In summary, we have found a macroscopic magnetic coupling phenomenon in a superconducting $YBa_2Cu_3O_{7-\delta}$ thin film. The coupling is between clusters of coupled vortices and the applied magnetic poles, each cluster containing millions of vortices. The coupling energy originates from the local-field inhomogeneity. To induce an effective coupling, the applied wavelength must be short enough, while the field amplitude must be strong. Compared with other methods, this finding largely increases the controlled vortex flow rate by several orders of magnitude. This finding has clearly explained the physical mechanism underlying the HTS flux pump, which provides inspiration and physical support for a new branch of wireless superconducting dc power sources, and tackles the PCM challenge for HTS magnets. This discovery offers opportunities over a wide range of applications such as in MRI, NMR, wind turbine, fusion, particle accelerator, and magnetically levitated trains, etc.

ACKNOWLEDGMENTS

This work was funded by the National Natural Science Foundation of China under Grant No. 51607117, the China Scholarship Council, and the Cambridge Overseas Trust. We gratefully acknowledge Professor Archie Campbell of Cambridge University for helpful discussions.

[1] E. H. Brandt, Vortex-vortex interaction in thin superconducting films, Phys. Rev. B **79**, 134526 (2009).
[2] C. P. Bean and J. D. Livingston, Surface Barrier in Type-II Superconductors, Phys. Rev. Lett. **12**, 14 (1964).
[3] W. Jung-Chun and Y. Tzong-Jer, Current distribution and vortex-vortex interaction in a superconducting film of finite thickness, Jpn. J. Appl. Phys. **35**, 5696 (1996).
[4] G. Carneiro and E. H. Brandt, Vortex lines in films: Fields and interactions, Phys. Rev. B **61**, 6370 (2000).
[5] J. Pearl, Current distribution in superconducting films carrying quantized fluxoids, Appl. Phys. Lett. **5**, 65 (1964).
[6] C. P. Bean, Magnetization of high-field superconductors, Rev. Mod. Phys. **36**, 31 (1964).
[7] J. E. Villegas, S. Savel'ev, F. Nori, E. M. Gonzalez, J. V. Anguita, R. García, and J. L. Vicent, A superconducting reversible rectifier that controls the motion of magnetic flux quanta, Science **302**, 1188 (2003).
[8] R. P. Feynman, *The Feynman Lectures on Physics* (Addison-Wesley, Reading, MA, 1963), Vol. I, Chap. 46.
[9] I. Giaever, Magnetic Coupling Between Two Adjacent Type-II Superconductors, Phys. Rev. Lett. **15**, 825 (1965).
[10] C. S. Lee, B. Janko, I. Derenyi, and A. L. Barabasi, Reducing vortex density in superconductors using the "ratchet effect," Nature (London) **400**, 337 (1999).
[11] J. F. Wambaugh, C. Reichhardt, C. J. Olson, F. Marchesoni, and F. Nori, Superconducting Fluxon Pumps and Lenses, Phys. Rev. Lett. **83**, 5106 (1999).
[12] B. Y. Zhu, F. Marchesoni, and F. Nori, Controlling the Motion of Magnetic Flux Quanta, Phys. Rev. Lett. **92**, 180602 (2004).
[13] D. Cole, S. Bending, S. Savel'ev, A. Grigorenko, T. Tamegai, and F. Nori, Ratchet without spatial asymmetry for controlling the motion of magnetic flux quanta using time-asymmetric drives, Nat. Mater. **5**, 305 (2006).
[14] S. Savel'ev and F. Nori, Experimentally realizable devices for controlling the motion of magnetic flux quanta in anisotropic superconductors, Nat. Mater. **1**, 179 (2002).
[15] I. Giaever, Flux Pinning and Flux-Flow Resistivity in Magnetically Coupled Superconducting Films, Phys. Rev. Lett. **16**, 460 (1966).
[16] M. D. Sherrill, Fluxon coupling in dual thin films, Phys. Rev. B **7**, 1908 (1973).
[17] P. R. Solomon, Voltage Associated with the Coupled Motion of Flux in Type-I Superconductors, Phys. Rev. Lett. **16**, 50 (1966).

[18] T. Pe, M. Benkraouda, and J. R. Clem, Magnetic coupling of two-dimensional pancake vortex lattices in a finite stack of thin superconducting films with transport currents in the two outermost layers, Phys. Rev. B **55**, 6636 (1997).
[19] R. Deltour and M. Tinkham, Coupled motion of vortices in superposed superconducting films, Phys. Rev. **174**, 478 (1968).
[20] P. E. Cladis, R. D. Parks, and J. M. Daniels, Phase Incoherence in the dc Superconducting Transformer, Phys. Rev. Lett. **21**, 1521 (1968).
[21] J. R. Manson and M. D. Sherrill, Fluxons in dual thin films, Phys. Rev. B **11**, 1066 (1975).
[22] M. D. Sherrill and W. A. Lindstrom, Superconducting dc transformer coupling, Phys. Rev. B **11**, 1125 (1975).
[23] J. W. Ekin, B. Serin, and J. R. Clem, Magnetic coupling in superposed type-II superconducting films, Phys. Rev. B **9**, 912 (1974).
[24] J. R. Clem, Theory of magnetically coupled type-II superconducting films, Phys. Rev. B **9**, 898 (1974).
[25] J. R. Clem, Theory of the coupling force in magnetically coupled type-II superconducting films, Phys. Rev. B **12**, 1742 (1975).
[26] W. Wang and T. Coombs, Magnetization of YBCO film with ac travelling magnetic waves of relatively short wavelengths, Appl. Phys. Lett. **110**, 072601 (2017).
[27] W. Wang, F. Spaven, M. Zhang, M. Baghdadi, and T. Coombs, Direct measurement of the vortex migration caused by traveling magnetic wave, Appl. Phys. Lett. **104**, 032602 (2014).
[28] W. Wang and T. A. Coombs, Vortex migration caused by travelling magnetic wave in a 2 in. diameter $YBa_2Cu_3O_{7-\delta}$ thin film, J. Appl. Phys. **113**, 213906 (2013).
[29] W. Wang and T. Coombs, The magnetisation profiles and ac magnetisation losses in a single layer YBCO thin film caused by travelling magnetic field waves, Supercond. Sci. Technol. **28**, 055003 (2015).
[30] W. Wang, M. Zhang, C. Hsu, and T. Coombs, Design consideration of a circular type magnetic flux pump device, IEEE Trans. Appl. Supercond. **22**, 5201304 (2012).
[31] W. Wang, M. Zhang, Z. Huang, Y. Zhai, Z. Zhong, F. Spaven, M. Baghdadi, and T. Coombs, Study of the penetration of a 2 inches diameter YBCO thin film with the travelling magnetic wave, IEEE Trans. Appl. Supercond. **24**, 4600304 (2014).
[32] W. Wang, R. Semerad, F. Spaven, M. Zhang, C. H. Hsu, Z. Zhong, Y. Chen, Z. Huang, and T. A. Coombs, The investigation of sweeping speed on the magnetization of a 2 inches diameter YBCO thin film with the circular-type magnetic flux pump, IEEE Trans. Appl. Supercond. **23**, 8201104 (2013).
[33] J. Gilchrist and M. Konczykowski, AC screening measurement for the characterization of oxide superconductors: I. Application to ceramics, Physica (Amsterdam) **168C**, 123 (1990).
[34] G. Fedor, Characterization of high-temperature superconductors by AC susceptibility measurements, Supercond. Sci. Technol. **10**, 523 (1997).
[35] J. l. G. Gilchrist, Penetration of time-varying fields into high-temperature superconductors, Supercond. Sci. Technol. **3**, 93 (1990).
[36] J. l. G. Gilchrist, Attenuation of rotating fields by superconducting screens, Supercond. Sci. Technol. **4**, 82 (1991).
[37] C. P. Bean, Rotational hysteresis loss in high-field superconductors, J. Appl. Phys. **41**, 2482 (1970).
[38] J. R. Clem and A. Perez-Gonzalez, Flux-line-cutting and flux-pinning losses in type-II superconductors in rotating magnetic fields, Phys. Rev. B **30**, 5041 (1984).
[39] A. A. Polyanskii, A. Gurevich, J. Jiang, D. C. Larbalestier, S. L. Bud'ko, D. K. Finnemore, G. Lapertot, and P. C. Canfield, Magneto-optical studies of the uniform critical state in bulk MgB_2, Supercond. Sci. Technol. **14**, 811 (2001).
[40] M. Motta, F. Colauto, T. H. Johansen, R. B. Dinner, M. G. Blamire, G. W. Ataklti, V. V. Moshchalkov, A. V. Silhanek, and W. A. Ortiz, Flux avalanches triggered by AC magnetic fields in superconducting thin films, Physica (Amsterdam) **479C**, 134 (2012).
[41] C. P. Bean, Magnetization of Hard Superconductors, Phys. Rev. Lett. **8**, 250 (1962).
[42] L. D. Cooley and A. M. Grishin, Pinch Effect in Commensurate Vortex-Pin Lattices, Phys. Rev. Lett. **74**, 2788 (1995).
[43] A. V. Silhanek, J. Gutierrez, R. B. G. Kramer, G. W. Ataklti, J. Van de Vondel, V. V. Moshchalkov, and A. Sanchez, Microscopic picture of the critical state in a superconductor with a periodic array of antidots, Phys. Rev. B **83**, 024509 (2011).
[44] C. Di Giorgio, F. Bobba, A. M. Cucolo, A. Scarfato, S. A. Moore, G. Karapetrov, D. D'Agostino, V. Novosad, V. Yefremenko, and M. Iavarone, Observation of superconducting vortex clusters in S/F hybrids, Sci. Rep. **6**, 38557 (2016).
[45] M. Z. Cieplak, Z. Adamus, M. Kończykowski, L. Y. Zhu, X. M. Cheng, and C. L. Chien, Tuning vortex confinement by magnetic domains in a superconductor/ferromagnet bilayer, Phys. Rev. B **87**, 014519 (2013).
[46] L. J. M. van de Klundert and H. H. J. ten Kate, Fully superconducting rectifiers and fluxpumps Part 1: Realized methods for pumping flux, Cryogenics **21**, 195 (1981).
[47] C. Hoffmann, D. Pooke, and A. D. Caplin, Flux pump for HTS magnets, IEEE Trans. Appl. Supercond. **21**, 1628 (2011).
[48] Z. Bai, G. Yan, C. Wu, S. Ding, and C. Chen, A novel high temperature superconducting magnetic flux pump for MRI magnets, Cryogenics **50**, 688 (2010).
[49] F. Lin, M. Koichi, L. Thibault, I. Yukikazu, and C. Tim, A flux pumping method applied to the magnetization of YBCO superconducting coils: Frequency, amplitude and waveform characteristics, Supercond. Sci. Technol. **29**, 04LT01 (2016).
[50] T. Nakamura, M. Sugano, T. Doi, and N. Amemiya, Flux pumping effect of HTS films in a traveling magnetic field, IEEE Trans. Appl. Supercond. **20**, 1033 (2010).
[51] A. M. Campbell, A finite element calculation of flux pumping, Supercond. Sci. Technol. **30**, 125015 (2017).
[52] C. W. Bumby, Z. Jiang, J. G. Storey, A. E. Pantoja, and R. A. Badcock, Anomalous open-circuit voltage from a high-T_c superconducting dynamo, Appl. Phys. Lett. **108**, 122601 (2016).
[53] Z. Jiang, K. Hamilton, N. Amemiya, R. A. Badcock, and C. W. Bumby, Dynamic resistance of a high-T_c superconducting flux pump, Appl. Phys. Lett. **105**, 112601 (2014).

[54] J. Geng, B. Shen, C. Li, H. Zhang, K. Matsuda, J. Li, X. Zhang, and T. A. Coombs, Voltage-ampere characteristics of YBCO coated conductor under inhomogeneous oscillating magnetic field, Appl. Phys. Lett. **108**, 262601 (2016).

[55] H. Seungyong, Linear flux pump: A potential alternative to energize superconducting magnet, Supercond. Sci. Technol. **29**, 070502 (2016).

[56] E. Pardo, Dynamic magneto-resistance: Turning a nuisance into an essential effect, Supercond. Sci. Technol. **30**, 060501 (2017).

[57] W. Wang, Y. Lei, S. Huang, P. Wang, Z. Huang, and Q. Zhou, Charging 2G HTS double pancake coils with a wireless superconducting DC power supply for persistent current operation, IEEE Trans. Appl. Supercond. **28**, 0600804 (2018).

Correction: The original Figures 2(a)–2(c) and Figures 3(a) and 3(b) contained plotting errors and have been replaced with the correct plots.